Boundary Current Eddies and Their Role in the Restratification of the Labrador Sea[*]

Caroline A. Katsman[+]

Woods Hole Oceanographic Institution, Woods Hole, Massachusetts, and Institute for Marine and Atmospheric Research Utrecht, Utrecht, Netherlands

Michael A. Spall and Robert S. Pickart

Woods Hole Oceanographic Institution, Woods Hole, Massachusetts

ABSTRACT

An idealized model is used to study the restratification of the Labrador Sea after deep convection, with emphasis on the role of boundary current eddies shed near the west coast of Greenland. The boundary current eddies carry warm, buoyant Irminger Current water into the Labrador Sea interior. For a realistic end-of-winter state, it is shown that these Irminger Current eddies are efficient in restratifying the convected water mass in the interior of the Labrador Sea. In addition, it is demonstrated that Irminger Current eddies can balance a significant portion of the atmospheric heat loss and thus play an important role for the watermass transformation in the Labrador Sea.

1. Introduction

The Labrador Sea is an area of high climatic importance with respect to the global meridional overturning circulation. Along its boundary flow waters originating from the Nordic and Arctic domains, as well as the recirculation of modified Gulf Stream water from the subtropics. These waters are modified locally by mixing as well as strong air–sea interaction. Deep convection in the Labrador Sea interior produces a mode water, Labrador Sea Water, that ventilates much of the North Atlantic Ocean at intermediate depths. Near the outer continental shelf and shelf break, the West Greenland and Labrador Currents transport Arctic-origin water equatorward (Fig. 1). Offshore of these currents, on the continental slope, resides a deep-reaching boundary current that transports the warm and salty waters of subtropical origin plus the Sverdrup return flow of the wind-driven subpolar gyre. For the purpose of this paper, we will refer to this slope flow as the Irminger Current. Farther offshore, near the bottom, dense overflow waters

from the Nordic seas are carried by the deep western boundary current.

During winter Labrador Sea Water (LSW) is formed in the interior of the sea, through modification of the surface waters by strong atmospheric forcing (Lazier 1973; Clarke and Gascard 1983). The formation of LSW is governed by many different factors, including the regional circulation and air–sea forcing, which is probably why it displays such pronounced interannual and interdecadal variability (Rhines and Lazier 1995; Dickson et al. 1996). In recent years, the focus of many modeling studies has been on the wintertime processes resulting in deep convection (e.g., Marshall and Schott 1999; Jones and Marshall 1993; Visbeck et al. 1996). In addition to these processes, the restratification after deep convection is of crucial importance for the formation of LSW in the subsequent year.

Hydrographic surveys along the World Ocean Circulation Experiment (WOCE) AR7W section (Fig. 1), generally occupied in the late spring or early summer season, have been done annually since 1989. After winters of deep-reaching convection, the newly formed LSW is found to be capped by a stratified layer of about 1000-m thickness in summer (Lilly et al. 1999). Time series from moorings near the location of former Ocean Weather Station (OWS) Bravo (Fig. 1) have revealed aspects of the evolution of this restratification process. The upper part of the water column rapidly becomes warmer and saltier after the convection ceases (Lilly et al. 1999). This generally occurs in late March, while the ocean is still cooled by the atmosphere, indicating that at least

---

Corresponding author address: Caroline A. Katsman, KNMI, Oceanographic Research Department, P.O. Box 201, 3730 AE De Bilt, Netherlands.
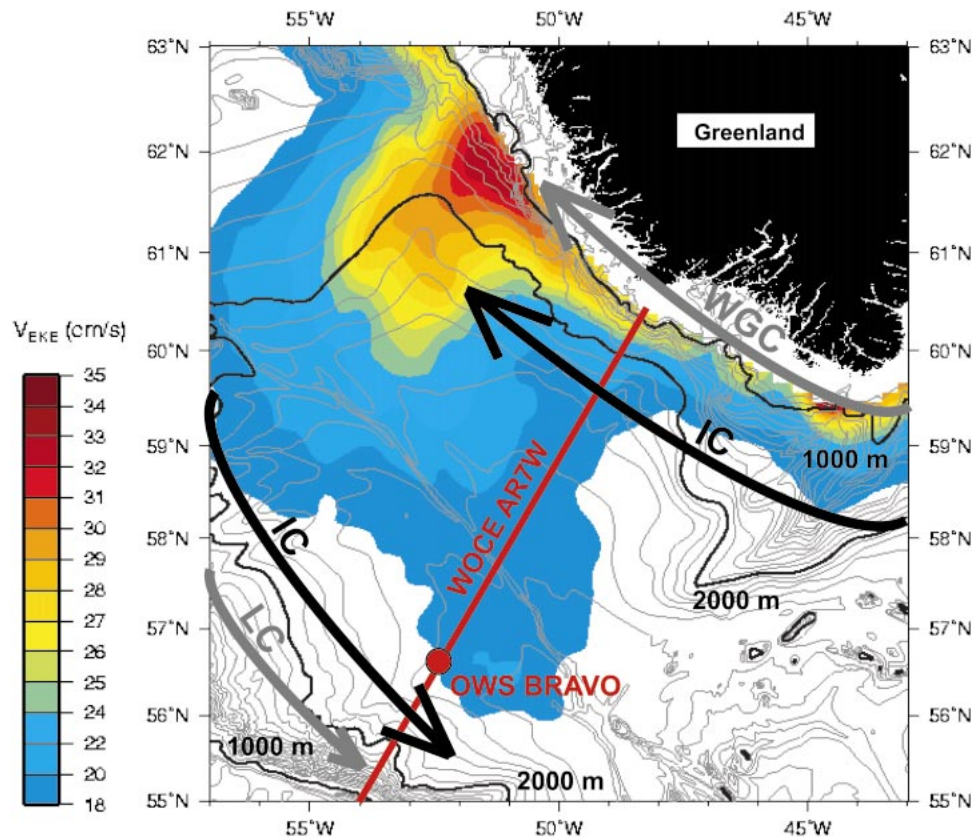E-mail: katsman@knmi.nl

FIG. 1. Map of the Labrador Sea region showing the bathymetry (thin gray and black lines), the location of former OWS Bravo (red circle), and the WOCE AR7W hydrographic section (red line). Colors depict the equivalent eddy speed V_{EKE} deduced from the sea surface height variability (from Lilly 2002). Arrows schematically depict the boundary current system on the continental shelf (gray; WGC: West Greenland Current; LC: Labrador Current) and slope (black; IC: Irminger Current).

part of the restratification is governed by oceanic processes.

The observational data are still too scarce to provide us with a clear view of the physical processes responsible for the restratification. However, the fact that it is rapid and deep reaching points to a mechanism involving lateral eddy fluxes. Two types of eddies may be important in this regard. Jones and Marshall (1997, hereinafter referred to as JM97) studied the restratification of an unstratified cylinder (meant to represent the end product of convection) embedded in a stratified environment with a high-resolution ocean model. At the front separating the stratified water from the convected water mass, a rim current develops in thermal wind balance with the lateral density gradient. Subsequently, this rim current becomes unstable and starts to shed geostrophic eddies that then efficiently restratify the convected cylinder. We will refer to this type of eddy as a rim current eddy.

A second type of eddy that may play a role in the restratification process is one that we will refer to as an Irminger Current eddy. Data from altimetry and surface drifters in the western North Atlantic Ocean show a region of enhanced variability in the Labrador Sea, close to the west coast of Greenland (e.g., White and Heywood 1995; Stammer and Wunsch 1999; Fratantoni 2001; Cuny et al. 2002; see Fig. 1). The amplitude of this signal displays a clear seasonal cycle, with a maximum in spring (White and Heywood 1995; Prater 2002). A growing amount of evidence suggests that this region of enhanced variance is associated with the formation of warm-core eddies from the Irminger Current, which flows along the perimeter of the basin (Lilly et al. 2003; Prater 2002). The formation of these eddies is apparently triggered by the local bathymetry (Eden and Böning 2002; Bracco and Pedlosky 2003). Along Greenland's west coast, the continental slope is narrower than along the rest of the coastline (Fig. 1), and the strongest variability is found at the downstream end of this constriction. The importance of topography and boundary current instabilities for the thermohaline circulation in marginal seas, and the restratification of deep convection in the interior, is discussed in a more general context by Spall (2004).

In this study we focus on the role of Irminger Current eddies in the rapid restratification of the Labrador Sea

after wintertime convection. We also investigate the relative importance of this process versus restratification via the rim current eddies studied by JM97. An idealized numerical model of the Labrador Sea region is used (section 2), which can simulate fairly realistic Irminger Current eddies (section 3). The unforced spindown problem discussed by JM97 is revisited in section 4 to contrast the role of Irminger Current eddies and rim current eddies. In section 5 we investigate whether the lateral heat transport provided by Irminger Current eddies is large enough to result in an equilibrated state, whereby this eddy transport balances the annual net heat loss from the Labrador Sea to the atmosphere.

2. Model configuration

The numerical simulations described in this paper were performed with the hydrostatic version of the Massachusetts Institute of Technology (MIT) primitive equation model (Marshall et al. 1997) in an idealized configuration of the Labrador Sea region. The computational domain and the bathymetry are shown in Fig. 2a. The basin is 930 km × 1350 km and rectangular, except in the northeast where a Gaussian peninsula representing the western portion of Greenland defines the edge of the domain. The maximum depth of the basin is 3000 m. A continental slope of varying width is defined along the perimeter except for the southern and eastern boundaries (the continental shelf is omitted). Of crucial importance for the formation of eddies in the Irminger Current is the narrowing of the slope along the west coast of Greenland, modeled after the observed constriction (Fig. 1, see also section 3b). South of the tip of Greenland an inflow is specified over a width of 150 km (see below); the remainder of the eastern boundary is closed. The outflow occurs in the southwest, over a 150 km wide portion of the southern boundary, where a radiation condition is applied to all variables (Orlanski 1976).

Unless otherwise stated, the simulations are performed for a horizontal grid size of 7.5 km and 15 levels in the vertical, and the β-plane approximation is used. Although in reality salinity also plays a role in determining the stratification of the Labrador Sea, we neglect its effect in this study for simplification and focus on the physical processes governing the restratification by considering temperature only. We use a linear equation of state $\rho = \rho_0(1 - \alpha T)$ with a reference density ρ_0 and a thermal expansion coefficient $\alpha = 2.0 \times 10^{-4}$ °C^{-1}. In most cases, the model is initialized with a spatially uniform stratification $T_{\text{ref}}(z)$, representative of the stratification in the western Labrador Sea in late summer. Subgrid-scale mixing is parameterized using Laplacian diffusion. The horizontal and vertical eddy viscosity and diffusion coefficients are $A_h = 40$ m^2 s^{-1} and $A_v = 1.0 \times 10^{-5}$ m^2 s^{-1}. At the solid lateral boundaries there is no heat flux and no normal flow.

The circulation is forced by specifying an inflow, representing the Irminger Current, at the eastern boundary. It is prescribed by means of a meridional temperature section T_{in} (y, z) and a westward flow U_{in} (y, z) in geostrophic balance with this temperature section:

$$T_{\text{in}}(y, z) = T_{\text{ref}}(z) + \frac{\Delta\rho}{2\alpha\rho_0}\left(1 - \frac{z}{z_b}\right)\left[1 + \tanh\left(\frac{y - y_0}{L_y}\right)\right]$$

(1a)

and

$$U_{\text{in}}(y, z) = \frac{g\Delta\rho}{4L_y f\rho_0}\frac{(z - z_b)^2}{z_b}\frac{1}{\cosh^2\left(\dfrac{y - y_0}{L_y}\right)},$$

(1b)

where z_b is the depth of the lowest level of the model, at which $U_{\text{in}} = 0$. A section across the inflow region is shown in Fig. 2b. The strength of the boundary current is determined by $\Delta\rho$ (the density difference across the boundary current) and its width L_y. The position of the current maximum is given by y_0. The standard parameter values used are $L_y = 22.5$ km, $y_0 = 22.5$ km south of the tip of Greenland, and $\Delta\rho = -0.3$ kg m^{-3} ($\Delta T = +1.5$°C). This results in a maximum westward inflow velocity of 0.65 m s^{-1}, in good agreement with the observed velocity over the upper continental slope of 0.60 m s^{-1} from surface drifters (Cuny et al. 2002). Estimates for the total transport of the current system around Greenland based on synoptic hydrographic sections range from 34 Sv (1 Sv $\equiv$ 10^6 m^3 s^{-1}) (Clarke 1984) to 50 Sv (Reynauld et al. 1995). A recent estimate by Pickart et al. (2002), which was derived using a combination of float data and repeat hydrographic sections, is 28.5 Sv for the total transport. The imposed transport at the inflow boundary (23.5 Sv) is in line with this latter estimate. Note, however, that the subsurface velocity maximum and transport associated with the deep western boundary current are not included in the definition of $U_{\text{in}}(z)$. Throughout this study, the conditions at the inflow boundary are kept constant. As an additional forcing, a surface heat flux $Q(x, y, t)$ is prescribed for the simulations presented in section 5. The exact forcing function will be described in that section. A simple convective adjustment scheme is applied to ensure vertical mixing of unstable density gradients, and there is no wind forcing in any of the model simulations.

3. Irminger Current eddies

In an extensive study, Lilly et al. (2003) made an inventory of the characteristics of eddies in the Labrador Sea, combining satellite altimetry and data from moorings deployed near the OWS Bravo site (marked by the red circle in Fig. 1). The latter data provided information on the horizontal and vertical structure of the eddies (Lilly et al. 1999, 2003). In the 5-yr observational record, 33 apparent eddies were identified (2 cyclones and 31 anticyclones). Twenty-five of those eddies could be
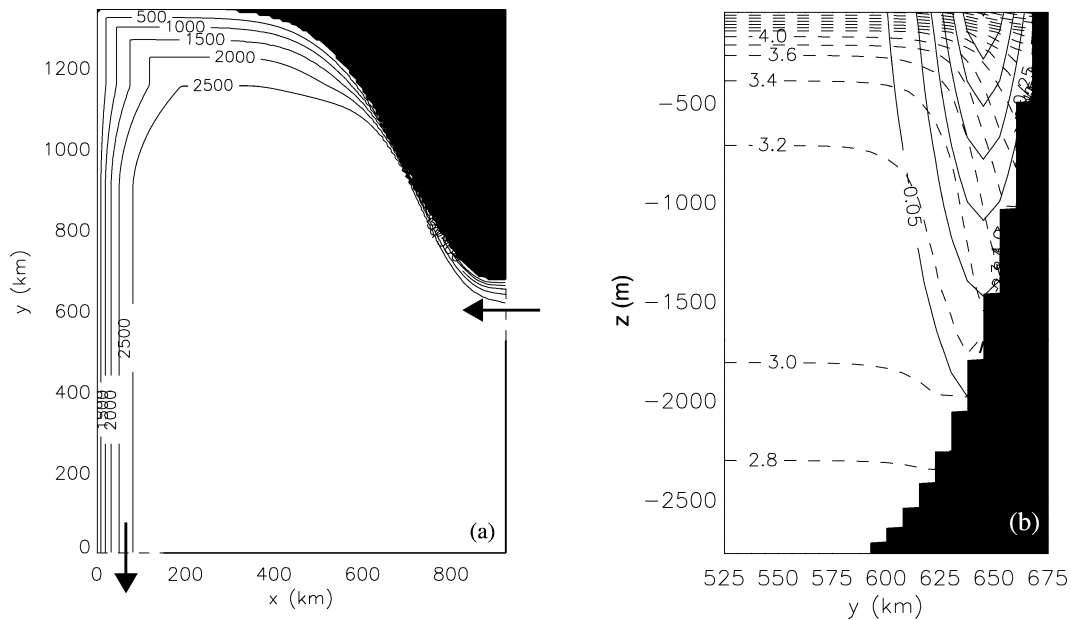
FIG. 2. (a) Model domain and bathymetry and (b) prescribed temperature (dashed; contour interval is 0.2°C) and westward velocity (solid; contour interval is 0.1 m s^{-1}) at the open portion of the eastern boundary.

classified as one of two distinct types; the 8 others were of a different or ambiguous type. The first type (13 eddies, or 39%) is an anticyclonic "convective lens": an eddy with a radius of 5–18 km, maximum surface velocity of about 0.15 m s^{-1}, and a relatively cold, fresh core at middepth. Based on these properties, Lilly et al. (2003) concluded that this type of eddy is formed during deep convection in the Labrador Sea. These convective lenses, which are too small and weak to be detected in the altimetry signal, appear similar in nature to the rim current eddies discussed in section 1.

The second type of eddy observed at the mooring site (12 eddies, or 36%) was termed an "Irminger eddy" by Lilly et al. (2003): a surface-intensified anticyclone with a radius of 15–30 km, surface velocity of 0.30–0.80 m s^{-1}, and a warm, salty core of water originating from the Irminger Current. The anomalous sea surface height signal associated with these eddies is large enough so that eddy events detected at the mooring site could be linked with simultaneous signals in the altimetry data. Using the latter, Lilly et al. (2003) deduced that the Irminger Current sheds 15–45 eddies each year, roughly divided into 40% anticyclones, 30% cyclones, and 30% dipoles. The apparent radius (the distance between the center of the eddy and its velocity maximum) is about 23 km. After formation, the eddies propagate southwestward into the Labrador Sea at a speed of about 0.05 m s^{-1} (~4 km day^{-1}). Farther into the basin, the ratio of cyclones to anticyclones decreases significantly. While in reality the Irminger Current eddies transport salt as well as heat, salinity effects are neglected entirely in this study for simplicity. This seems justified since observations show that the eddy structure is dominated

by temperature effects, both in summer ($\alpha\Delta T/\beta\Delta S \sim 5$; Lilly and Rhines 2002, their Fig. 9b) and winter (Pickart et al. 2002, station 92 in their Figs. 8a–c).

Eden and Böning (2002) reproduced the observed region of enhanced variability near the west coast of Greenland in a high-resolution ocean circulation model. In their simulation, anticyclonic Irminger Current eddies are spawned at the downstream end of the constriction in the bathymetry (see Fig. 1). These eddies are surface intensified (velocities up to 0.45 m s^{-1}) and have a warm, saline core down to a depth of about 1000 m. Few cyclones are generated, and these are generally weaker and have a more depth-independent structure. Eden and Böning's eddy field seems to be in good agreement with the available observations (Lilly et al. 2003; Prater 2002). Using the much simpler model configuration introduced in section 2, it is also possible to generate fairly realistic Irminger Current eddies. We first focus on the characteristics of the simulated Labrador Sea eddy field and on sensitivity of the eddy formation to the bathymetry. In subsequent sections, we will turn to the role of these eddies in the restratification of the Labrador Sea.

a. Characteristics of the simulated eddy field

The simulated eddy field is studied based on a 3-yr simulation of the boundary current (section 2) without any surface forcing. As an example, a snapshot of the eddy field is shown in Fig. 3a. To obtain a good impression of their life cycle, the eddies were tracked visually over the first 180 days of the simulation using such snapshots. After an initial spinup period of about
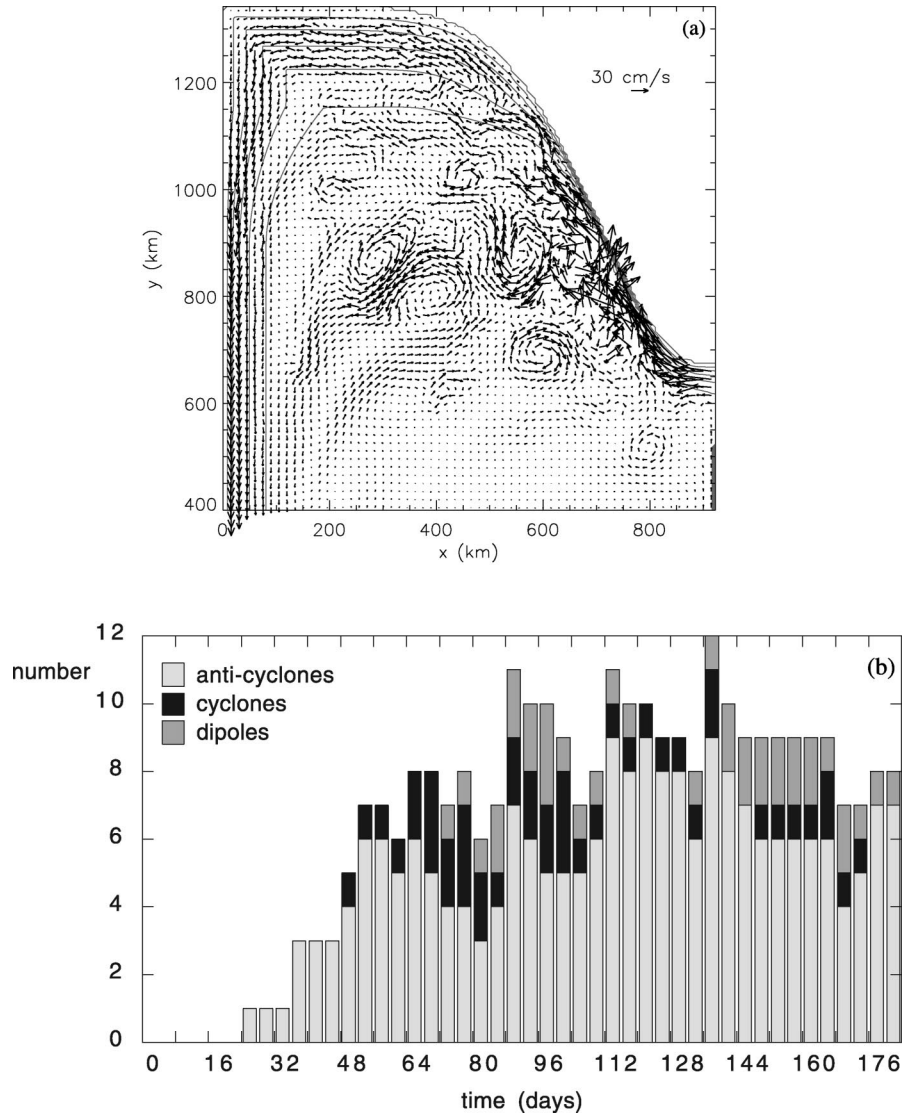
FIG. 3. (a) Snapshot of the near-surface velocity on day 150. Arrows are shown at every other grid point for clarity; contours show the bathymetry (contour interval is 500 m; $y > 400$ km). Several anticyclones and a dipole are clearly visible. (b) Histogram showing the number of identified anticyclones (light gray), cyclones (black), and dipoles (dark gray) as a function of time during the first 180 days of the simulation.

two months, on average 8–9 eddies can be identified in the Labrador Sea at any given time. In total, 35 eddies were formed during the first 180 days of the simulation. The majority of these eddies are anticyclones, but cyclones and dipoles are also present, as seen in the histogram of Fig. 3b. About 45% of the tracked eddies (16 out of 35) exist for less than two weeks (they spin down, merge with other eddies, or are recaptured by the boundary current) and/or have weak surface flows (<0.3 m s^{-1}). The algorithm used by Lilly et al. (2003) to identify eddies in the altimetry data requires a minimal anomalous sea surface height signal of 10 cm and so such features would probably be excluded. Therefore, we focus on the 19 long-lived, strong eddies that are

shed, of which 15 are anticyclones and 4 are cyclones when they first emerge. The interactions between the eddies in the Labrador Sea interior were numerous and varied. During the simulation, examples were seen of anticyclones and cyclones merging into dipoles, anticyclones developing into dipoles, and splitting and merging anticyclones.

The average radius of the eddies is about 25 km, in agreement with the altimetry data (Lilly et al. 2003). The depth-averaged temperature anomaly ΔT of the newly formed anticyclones with respect to the background stratification T_{ref}, representing summer conditions in the Labrador Sea, is $\Delta T = 0.25°C$ over 3000 m. Hydrographic observations of Irminger Current eddies near
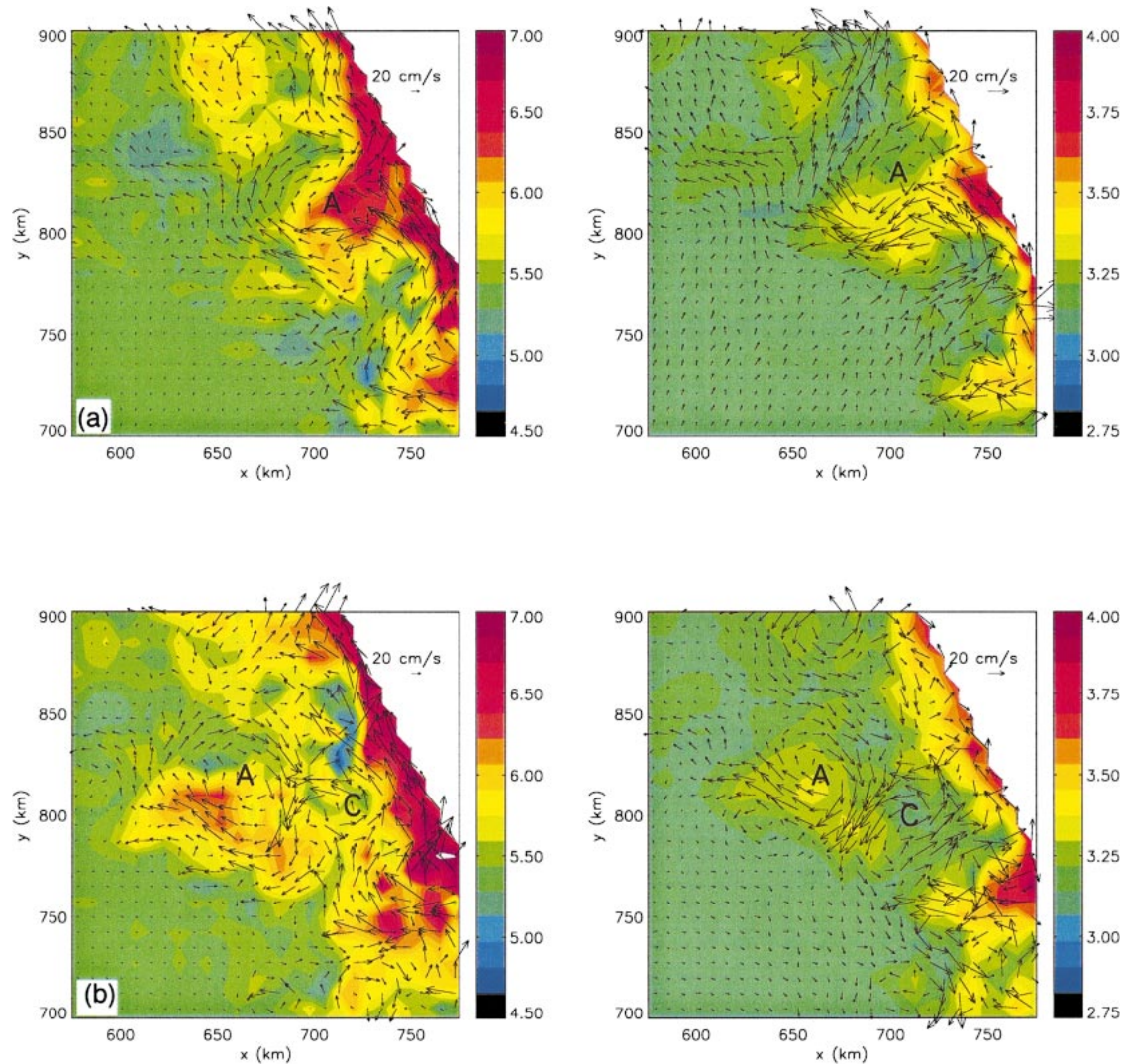
FIG. 4. Shedding of an anticyclone from an Irminger Current meander. Shown are temperature (°C; colors) and velocity (arrows) for the (left) near-surface flow and the (right) flow at 1200-m depth. The snapshots in (a) and (b) are four days apart.

the west coast of Greenland are relatively rare, consisting mainly of occasional vertical profiles obtained during the routine survey of the WOCE AR7W section. An example of such an observation is an anticyclonic eddy sampled during the occupation of the section in June/July 1998. The depth-averaged temperature anomaly of this eddy with respect to the average temperature along the section during that same survey is about $\Delta T = 0.3°C$ over 3000 m. The vertical structure of the modeled anticyclones thus seems reasonable.

The anticyclonic eddies develop from meanders of the Irminger Current. An example of a shedding event appears in Fig. 4, through velocity (arrows) and temperature fields (colors) near the surface and at 1200-m depth (the center of the anticyclone is marked by A). Often, a cyclonic circulation develops at the upstream end of the meander (marked C in Fig. 4), akin to the near-field circulation of opposite vorticity seen near de-

veloping meanders in baroclinically unstable open-ocean jets (Bush et al. 1996). This is particularly clear at depth (right panels), where the developing eddy has a dipolar structure. The anticyclones contain warm boundary current water, while the adjacent cyclones have the same temperature structure as the water in the interior. The few isolated cyclones that are observed in the model all seem to form as a result of interactions between an anticyclone and the Irminger Current or between two neighboring anticyclones, rather than being shed directly from the Irminger Current. As a consequence, the cores of the cyclones generally do not contain Irminger Current water.

After being shed, eddies generally move southwestward into the Labrador Sea interior (Fig. 5). Their tracks are strongly affected by the presence of the Irminger Current and other eddies nearby (several splitting and merging events can be identified in Fig. 5). On average,
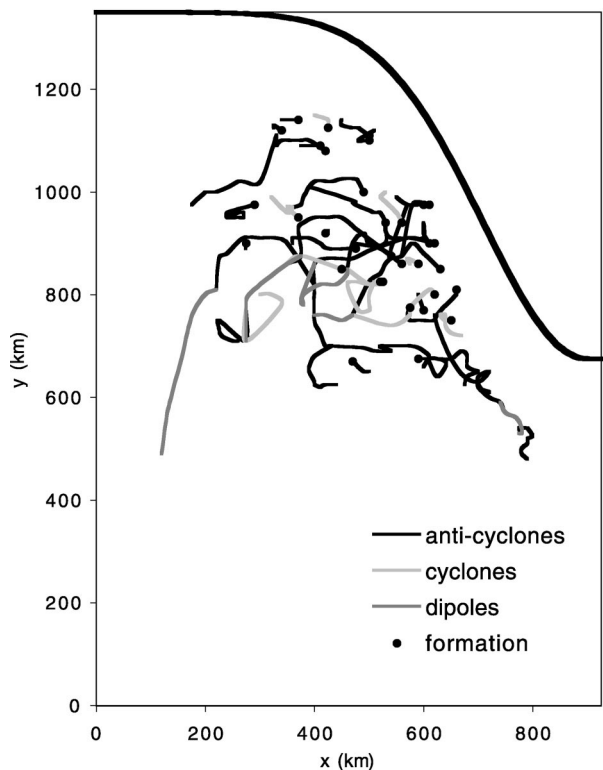
FIG. 5. Paths of the 35 eddies tracked during the first 180 days of the simulation. Different line styles indicate the polarity of the eddies (see legend), and circles mark their formation location.

FIG. 6. Smoothed surface EKE calculated over days 100–1080 of a 3-yr simulation of the unstable Irminger Current (contour interval is 25 cm^2 s^{-2}). Only the northern part of the domain ($y > 400$ km) is shown; gray contours denote the bathymetry (contour interval is 500 m).

the propagation speed of the eddies is 0.06 m s^{-1}, in line with the value of 0.05 m s^{-1} derived from the altimeter data (Lilly et al. 2003). Instantaneous eddy propagation speeds can be as large as 0.2 m s^{-1} for shorter periods.

The surface eddy kinetic energy EKE of the simulated eddy field, defined as

$$\mathrm{EKE} = \frac{1}{2}(\overline{u'^2 + v'^2})$$

(where the overbar denotes time averaging and primed variables are deviations from the time mean), is analyzed using velocity fields from the 3-yr simulation of the unstable Irminger Current from day 100 onward. A localized EKE maximum of about 300 cm^2 s^{-2} is found near the west coast of Greenland (Fig. 6). Farther away from the coast, the eddy activity decays rapidly. The spatial pattern is similar to the observations (Fig. 1), and its magnitude lies within the reported range of 200–500 cm^2 s^{-2} (White and Heywood 1995; Stammer et al. 2001; Fratantoni 2001; Prater 2002; Lilly et al. 2003; Cuny et al. 2002).

b. Sensitivity of the eddy formation to the local bathymetry

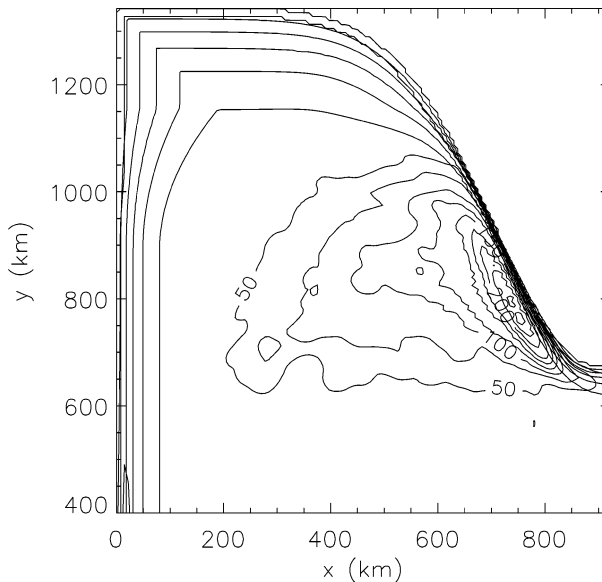The localization of the EKE maximum at the downstream end of the constriction (Fig. 1) suggests that the local bathymetry is important for the formation of Irminger Current eddies. It is unclear, however, whether the eddy formation process is governed by the conditions at the downstream end of the constriction or whether the instabilities are triggered at the upstream end and grow in size and/or strength while propagating toward the downstream end.

Based on an analysis of the energy conversion rates in the upper 500 m of the water column, Eden and Böning (2002) found a maximum in the conversion from mean to eddy kinetic energy (which can be associated with barotropic instability) at the upstream end of constriction, on the continental slope. This instability is attributed to the local sharpening of the boundary current as it is steered by the steep bathymetry, resulting in high horizontal shear. On the continental shelf, baroclinic energy conversions of comparable magnitude are found. By contrast, Bracco and Pedlosky (2003) showed that a purely baroclinic current in a zonal channel, which is unstable over an interval of limited extent due to the local steepness of the bathymetry, gives rise to the formation of both anticyclones and cyclones near the coast. While the cyclones remain trapped in the area with steep bathymetry, the anticyclones move downstream along the coast. As was noted by the authors, this behavior qualitatively resembles that of Irminger Current eddies in the Labrador Sea, thus suggesting that the eddy formation mechanism might be baroclinic.

As in Eden and Böning (2002), we use the expression for the baroclinic and barotropic energy conversion rates for an unbounded open domain presented by Böning and Budich (1992) to diagnose the energy conversions
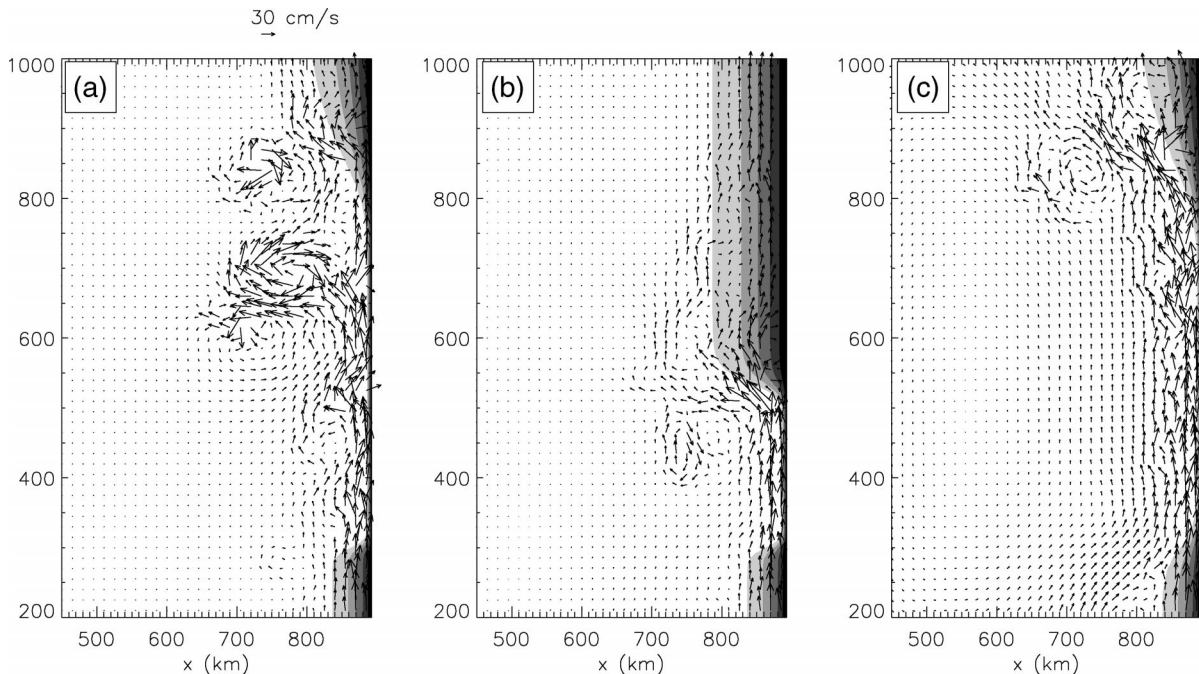
FIG. 7. Near-surface velocity on day 60 for various sensitivity experiments in a meridional channel (only the vicinity of the constriction is shown): (a) the standard constriction, (b) a constriction of limited extent, and (c) a constriction with a wide transition region. Gray shading shows the bathymetry; vectors are shown at every other grid point.

in our simulation. The results show that the instability process is mixed: the barotropic energy conversion rate is more important in the upper water column, while the baroclinic energy conversion rate is largest at mid-depths. Both terms show a maximum at the upstream end of the constriction in the bathymetry.

The energy analysis motivates further exploration of the effects of the extent and shape of the constriction in the bathymetry on the eddy shedding process, in particular at its upstream end. The standard bathymetry of the model, although idealized compared to reality, is still fairly complex. Therefore, a series of short simulations was performed using a meridional channel of 900 km × 1200 km on an f plane, with 150-km-wide inflow and outflow regions in the southeast and northeast, respectively, and a slope along its eastern boundary (Fig. 7). The topography is exponential in the zonal direction and has an e-folding scale that varies in the meridional direction. The shape of the constriction is governed by three length scales: (i) the e-folding scale defining the steepness of the slope at the constriction, (ii) the meridional extent of the constriction, and (iii) the width of the transition region between the wide and the steep slope.

The constriction displayed in Fig. 7a uses length scales comparable to those found near the west coast of Greenland. For this case the boundary current starts to meander as soon as it encounters the steep part of the slope. Eddies are shed near $y = 700$ km and then move westward. When the e-folding scale of the topography

at the constriction is doubled, the boundary current remains stable (not shown). For the shedding of isolated eddies from the boundary current it is not only required that the local slope is sufficiently steep, but also that it is steep over a considerable meridional extent: as long as the downstream end of the constriction lies north of the preferred location for eddy shedding ($y \simeq 700$ km), eddies are still generated. Otherwise, the boundary current does start to meander but these meanders do not evolve into isolated eddies (Fig. 7b). The conditions at the upstream end of the constriction apparently govern the growth rate of the instabilities: when the width of the transition region at this upstream end is increased (Fig. 7c), less and generally weaker eddies are shed. Sensitivity experiments with variations on the standard bathymetry (Fig. 2a) support the results from these highly idealized channel simulations.

4. Restratification after deep convection

Now that it has been established that the characteristics of the simulated eddy field are in reasonable agreement with the observations, we turn to the role of Irminger Current eddies in the restratification of the Labrador Sea after deep convection. Spindown experiments were performed to study the evolution of a realistic end-of-winter state in the absence of surface forcing, with and without an eddy-shedding boundary current. This way the contribution of the boundary current eddies

versus the interior rim current eddies to the restratification of the Labrador Sea can be assessed.

a. Restratification by rim current eddies

Besides presenting spindown experiments of the restratification of an unstratified cylinder embedded in a stratified environment, JM97 also derived an estimate for the time needed to restratify the convected water mass and applied it to the Labrador Sea. One can assume that, in the absence of surface heat flux, changes in the buoyancy $\overline{b}$ of the mixed cylinder are due to eddy fluxes $\overline{v'b'}$ across the front that initially separates the convected fluid from the stratified water mass:

$$\frac{\partial}{\partial t} \int \overline{b} \, dV = 2\pi r \int \overline{v'b'} \, dz, \tag{2a}$$

where the integrals are over the volume and the sides of the cylinder, respectively. The buoyancy fluxes $\overline{v'b'}$ are provided by geostrophic eddies that grow on the rim current that develops along the front and becomes unstable. These rim current eddies are clearly present in the numerical simulations by JM97, who use convected cylinders of 20–100-km radius. The eddy fluxes are parameterized as

$$\overline{v'b'} = c_e \Delta b(z) u_0, \tag{2b}$$

where $\Delta b(z)$ is the initial buoyancy difference between the mixed cylinder and the ambient fluid, u_0 is the strength of the baroclinic rim current at the surface, and c_e is an efficiency constant deduced from the numerical simulations (JM97). After some manipulation of (2a) and making use of (2b), the restratification time scale τ can be estimated:

$$\tau = \frac{3}{2c_e} \frac{L_f}{L_d} \frac{r}{Nh}, \tag{2c}$$

where N is the stratification of the ambient fluid, h is the height of the convected cylinder, and r is its radius.

In this derivation, we have allowed for the width of the front L_f to differ from the deformation radius L_d. If $L_f = L_d$, as assumed by JM97, then (2c) reduces to their (2.11). The initial state used by JM97 indeed has a narrow front for which L_f is comparable to L_d (at high latitudes, $L_d = 10$–15 km). It represents the end product of convection induced by the application of a localized heat flux over a disk of a chosen radius [Jones and Marshall (1993) studied the convection process using this type of surface forcing]. Although the surface heat flux over the Labrador Sea is nonuniform, such an extreme localization seems unrealistic. Indeed, the convected region present in the Labrador Sea at the end of winter is not surrounded by such a narrow front, as was shown by Pickart et al. (2002, their Fig. 12d). Rather, L_f is about an order of magnitude larger than L_d [$L_f = O(100)$ km]. In addition, the wintertime observations show that the convected region is wider than the cylinder

of 20–100-km radius used by JM97 [$r = O(300)$ km]. As a consequence, we estimate the restratification time scale τ to be much larger than the value given by JM97. Using parameter values representative of the Labrador Sea ($L_f = 100$ km, $r = 300$ km, $L_d = 10$ km, $N = 1.5 \times 10^{-3}$ s^{-1}, and $h = 1000$ m) and $c_e = 0.027$, the restratification time τ is 3.5 yr. Here, we have assumed the same value for the efficiency constant c_e as JM97 since it has been found to be remarkably constant over a wide range of numerical experiments (Marshall and Schott 1999). Our estimate for τ is much larger than the observed restratification time scale at the OWS Bravo site (Lilly et al. 1999). Obviously, when the convected region is wider, a larger volume of water needs to be restratified. In addition, when L_f is larger, the rim current is weaker and less unstable (using the parameter values above, the strength of the rim current is 6 cm s^{-1}, rather than 60 cm s^{-1} as found in JM97). Direct velocity measurements in the Labrador Sea interior in winter are quite noisy and show no sign of strong, coherent rim currents (Pickart et al. 2002), more in line with our estimate than with that by JM97. While the mechanism for restratification proposed by JM97 may effectively restratify mixed patches of smaller scale (Marshall and Schott 1999), we hypothesize that the formation of rim current eddies is not the dominant mechanism responsible for the rapid large-scale restratification of the Labrador Sea after deep convection.

Spindown experiments for which the model is initialized with a convected region modeled after the observed state of the Labrador Sea at the end of winter (Fig. 8) confirm this. As in JM97, the front separating the convected region from the stratified waters is circular, but the convected region is cone shaped rather than cylindrical. The radius of the convected cone is 300 km at the surface and the maximum mixed layer depth is 1500 m. The width of the front surrounding the convected water is much larger than the Rossby deformation radius. The evolution of this initial state was monitored for a year, in the absence of any surface forcing.

First, a simulation without the warm boundary current was performed so that the convected region can only be restratified by eddies developing on the rim current along the surrounding front. Near-surface temperature plots after 60 and 120 days (Figs. 9a,b) clearly show eddy activity, but it is limited to a band of about 150 km around the original front and does not reach the interior of the convected region. The bulk of the convected cone remains much colder than the ambient water. The grid point at the center of the convected region, marked by an asterisk in Fig. 9, serves as the model equivalent of the OWS Bravo site. Here, the surface temperature increases only by 0.06°C in a year, due to diffusion rather than lateral fluxes provided by rim current eddies. Only a weak baroclinic rim current develops: its maximum velocity is $u_0 = 8$ cm s^{-1} averaged over the first two weeks, so in line with the theoretical
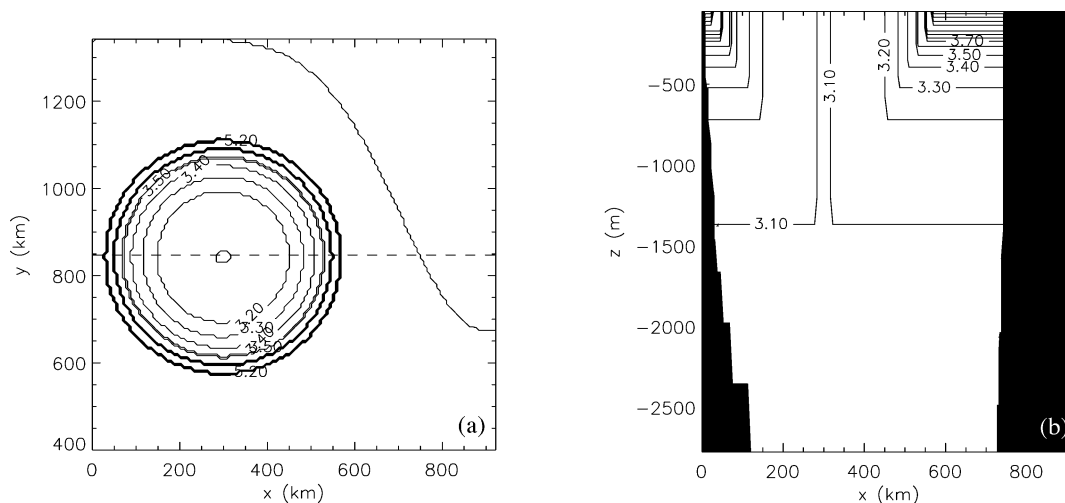
FIG. 8. Initial condition for the spindown simulations: (a) near-surface temperature field and (b) zonal section of temperature through the center of the convected region [dashed line in (a)]. Contour interval is 0.1°C (0.3°C) for $T <$ ($\geq$) 4°C.

estimate presented above, and decreases with time. By evaluating the temperature change near the front, one can directly estimate the efficiency constant c_e in (2b). In the narrow band where the eddies are active, the surface temperature changes by 0.8°C over the year (at deeper levels, the temperature change is smaller). Using (2a) and (2b) it follows that for this simulation $c_e = 0.02$, so similar to the value of $c_e = 0.027$ obtained by JM97.

When an initial state with a narrow front ($L_f \sim L_d$) is used, a stronger baroclinic current develops ($u_0 = 18$ cm s^{-1} averaged over the first two weeks). As a consequence, the eddy activity is more vigorous, but it is still limited to the frontal region (not shown). The sensitivity of the results to the lateral diffusion was considered briefly by repeating the spindown experiment on a horizontal grid of 5 km with $A_h = 20$ m^2 s^{-1} (recall that for the standard cases a grid size of 7.5 km and $A_h = 40$ m^2 s^{-1} were used). Minor quantitative changes occurred, but the cross-frontal eddy fluxes still act on a length scale of about 150 km, so that the central part of the convected region is not restratified after a year.

b. Restratification by Irminger Current eddies

In a second spindown experiment, the same setup was used except for the prescription of a warm Irminger Current, which becomes unstable and starts to shed eddies near the west coast of Greenland (see section 3). In this case, rapid restratification of the convected region does occur. Figures 9c and 9d clearly show the penetration of warm boundary-current water into the interior from the east. This lateral heat transport is provided by westward traveling anticyclonic Irminger Current eddies. One also sees that some of the convected water is transported southward with the boundary current. From

a time–depth plot at the grid point at the center of the convected region (Fig. 10) it is clear that the temperature increase is not limited to the surface but extends to a depth of 1000 m. In a year the surface temperature at this location increases by 2.6°C to a value that lies between that of the boundary current and that of the ambient, unconvected water at that depth. At 1000 m, the temperature increases by 0.2°C over a year.

The time span between the start of this simulation and the onset of the restratification (Fig. 10) is set by the spinup time of the boundary current and the propagation speed of the Irminger Current eddies. The first eddies are shed after about 20 days (Fig. 3b), after which it takes approximately 80 days to reach the chosen grid point. In reality, the Irminger Current eddies are present year round and so the onset of the restratification after deep convection is more rapid than is found for this spindown calculation. This is demonstrated in the following section by multiyear calculations with a seasonal heat flux forcing.

5. Equilibrium between surface cooling and eddy heat transport

In the previous section it was shown that Irminger Current eddies are far more efficient than rim current eddies in restratifying a convected region similar to that observed in the Labrador Sea at the end of winter. The question then arises as to whether the lateral heat transport by the Irminger Current eddies can compensate a substantial part of the net heat loss to the atmosphere that occurs over the basin. We address this question here in two ways: first by estimating this heat transport based on observations and second by means of a 10-yr model integration of the Irminger Current in combination with a fairly realistic surface heat flux.
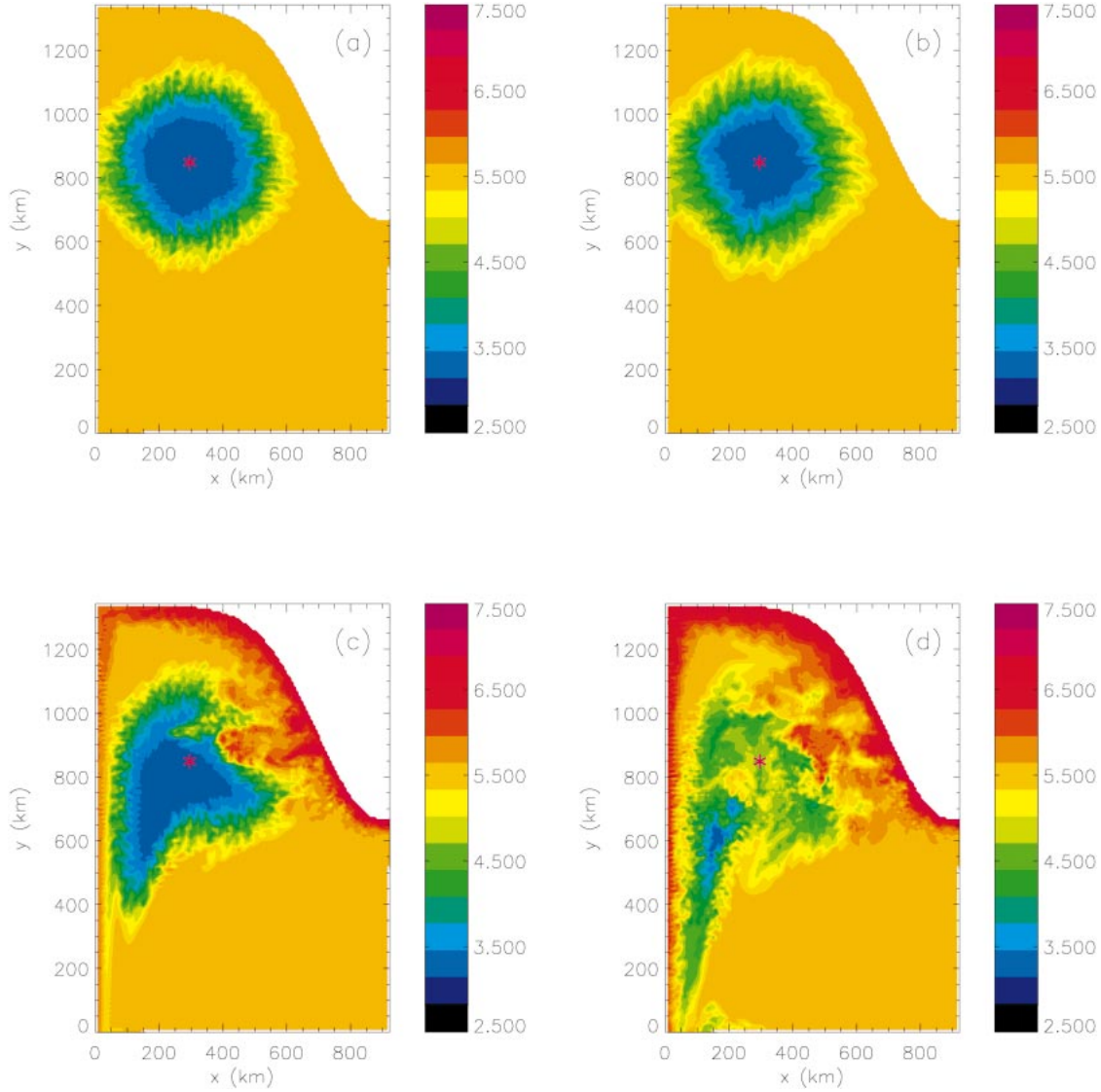
FIG. 9. Near-surface temperature (°C) for the spindown simulations (a), (b) without and (c), (d) with the unstable boundary current. Shown are snapshots at (left) day 60 and (right) day 120 of the simulations. An asterisk marks the center of the initial convected region and serves as the model equivalent of the OWS Bravo site.

a. Lateral heat transport by Irminger Current eddies

Averaged over the year, the heat flux out of the Labrador Sea is about $\overline{Q} = 30$–50 W m^{-2} (Smith and Dobson 1984; Lilly et al. 1999). This heat flux amounts to a total heat loss of

$$H_{\text{atm}} = \pi r_{\text{LS}}^2 \overline{Q} = 1.2\text{–}1.9 \ (10^{13} \ \text{J s}^{-1})$$

$$= 3.6\text{–}6.1 \ (10^{20} \ \text{J yr}^{-1}), \tag{3a}$$

assuming that the Labrador Sea is a circular basin of $r_{\text{LS}} = 350$ km radius. The heat content of a single Irminger Current eddy is estimated using

$$H_e = \pi r_e^2 \rho_0 c_p \int (T_e - T_{\text{bg}}) \ dz$$

$$= \pi r_e^2 \rho_0 c_p \int \Delta T \ dz, \tag{3b}$$

with r_e the radius of the eddy, ρ_0 a reference density, and c_p the heat capacity. In (3b), ΔT denotes the difference between the temperature of the eddy T_e and the background temperature T_{bg}. To estimate this temperature difference, temperature profiles from surveys of the WOCE AR7W section (Fig. 1) are used. For T_e, we use the temperature profile at a station inside an eddy sampled during the occupation of the section in June/July
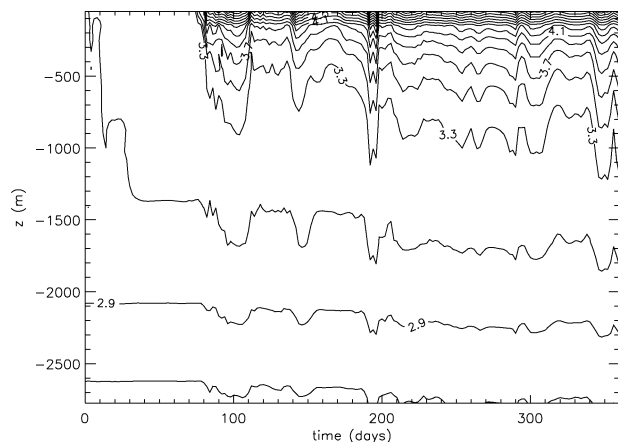
FIG. 10. Time–depth plot of temperature at the grid point at the center of the convected region (asterisk in Fig. 9) for the spindown simulation with a warm boundary current (contour interval is 0.2°C).

$$\overline{\Delta T} = \frac{1}{D} \int_0^D \Delta T \, dz = 0.57°\text{C}$$

over $D = 2500$ m. Using $r_e = 2.5 \times 10^4$ m, $\rho_0 = 1.0 \times 10^3$ kg m^{-3}, and $c_p = 4.0 \times 10^3$ J (kg °C)$^{-1}$, (3b) yields

$$H_e = \pi r_e^2 \rho_0 c_p \overline{\Delta T} D = 1.1 \times 10^{19} \text{ J}. \qquad (3c)$$

Assuming that roughly 30 eddies are shed each year, as reported by Lilly et al. (2003), (3c) implies that 55%–92% of the heat loss to the atmosphere in (3a) can be compensated by the Irminger Current eddies.

Lilly et al. (2003) also presented an estimate for the lateral heat transport by the Irminger Current eddies. However, they concluded that the eddies can account for only 28%–55% of the required heat transport. The discrepancy between the two estimates results from the definition of the heat anomaly $\overline{\Delta T}$ of the eddies that is used. For this Lilly et al. (2003) use the difference between T_e (Fig. 11a) and the average temperature profile from the AR7W survey of 1998. That is, they use a late spring/early summer occupation rather than a winter occupation to define T_{bg}. The OWS Bravo mooring data (Lilly et al. 1999) show that, at that time of the year, the restratification process is already well under way (temperatures are roughly halfway between their winter minimum and summer maximum). Hence, the heat content of the Irminger Current eddies is underestimated by roughly a factor of 2.

1998 (I. Yashayaev 2003, personal communication; Fig. 11a). The background temperature profile T_{bg} is based on the winter data presented by Pickart et al. (2002), since this winter state is the state that arises as a consequence of the net heat loss to the atmosphere and needs to be restratified over summer. Here T_{bg} is defined as the average over the 13 stations deeper than 3500 m along the AR7W section occupied in the winter of 1997 (Fig. 11a). The depth-averaged temperature anomaly $\overline{\Delta T}$ (Fig. 11b) calculated from these profiles is
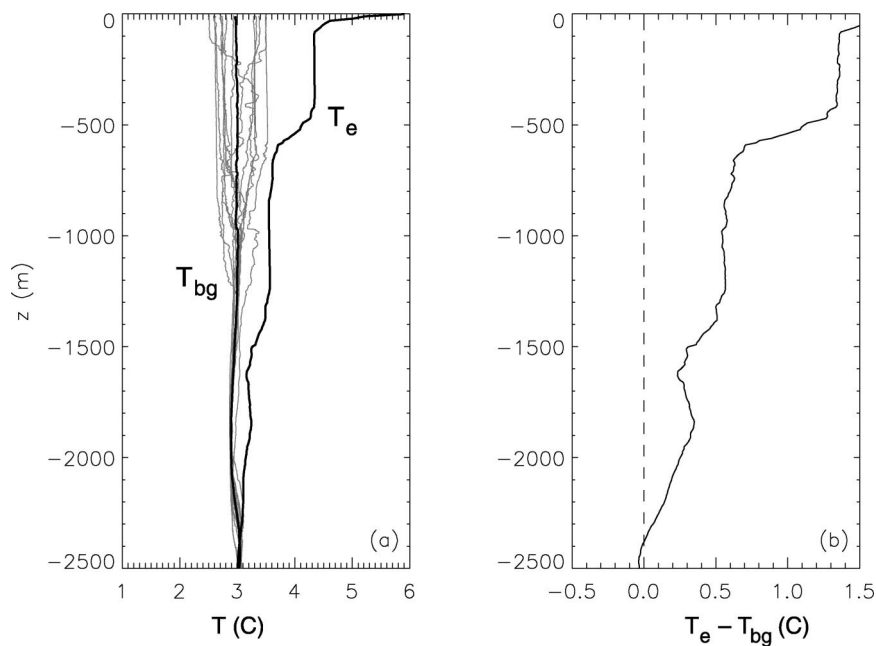

FIG. 11. Vertical temperature profiles from surveys of the WOCE AR7W section used to estimate the lateral heat transport by Irminger Current eddies. (a) Profiles from the 13 stations deeper than 3500 m from the winter of 1997 (gray lines), their average T_{bg}, and the temperature T_e of the eddy sampled in the summer of 1998. (b) Temperature anomaly $\Delta T = T_e - T_{bg}$.
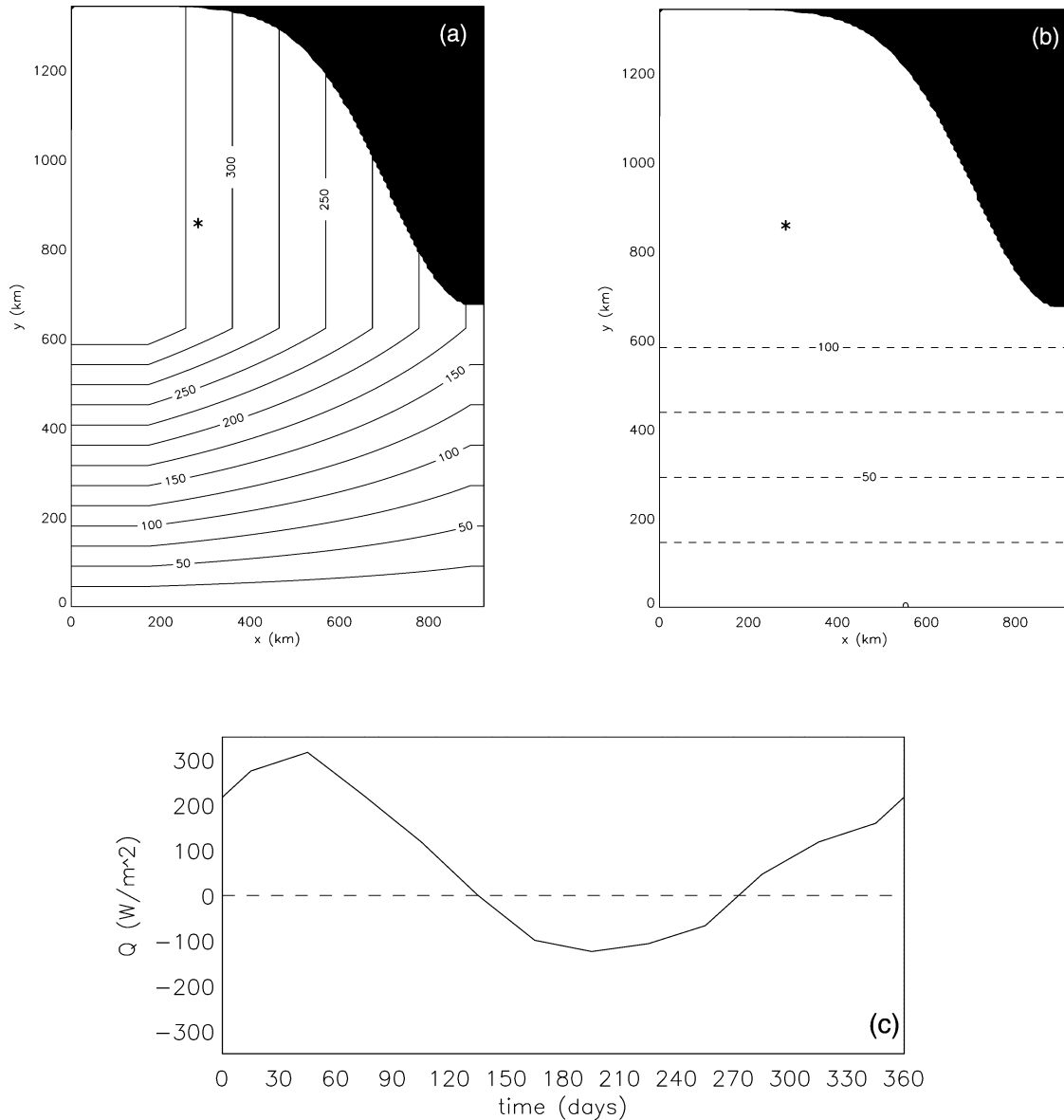
FIG. 12. Spatial pattern for the surface heat flux in (a) mid-Feb and (b) mid-Aug [contour interval is 25 W m^{-2}; and solid (dashed) contours denote a positive (negative) heat flux out of (into) the ocean]. The time dependence of the amplitude of the heat flux at the Bravo site [asterisk in (a) and (b)] is shown in (c).

b. Equilibration in the model simulations

Ten-year model simulations were performed to investigate whether a realistic equilibrated state can develop when the model forcing consists of a time-varying surface heat flux combined with an eddy-shedding boundary current. In winter, the outgoing heat flux ($Q > 0$) is prescribed to be strongest on the northwestern side of the basin (Fig. 12a), as observed (e.g., Sathiyamoorthy and Moore 2002). In the south Q ramps down linearly to avoid large heat fluxes near the (open) southern boundary for numerical reasons. In the northwest the maximum heat flux over the year is $Q = +345$ W m^{-2} in mid-February. During the short summer (Q

< 0), the heat flux into the ocean is assumed to be uniform in the northern part of the domain, and again to decrease toward the southern boundary (Fig. 12b). In mid-August, the maximum downward heat flux is $Q = -105$ W m^{-2}. The amplitude of the heat flux at the OWS Bravo site (asterisk in Figs. 12a,b) is modeled after data (Pickart et al. 1997, their Fig. 7), and is shown in Fig. 12c. The net outgoing heat flux over the entire domain is $\overline{Q} = +43$ W m^{-2}, within the range of observations (Smith and Dobson 1984; Lilly et al. 1999). The Irminger Current is prescribed at the inflow boundary as before, and the initial stratification is spatially uniform and equal to T_{ref} (section 2).
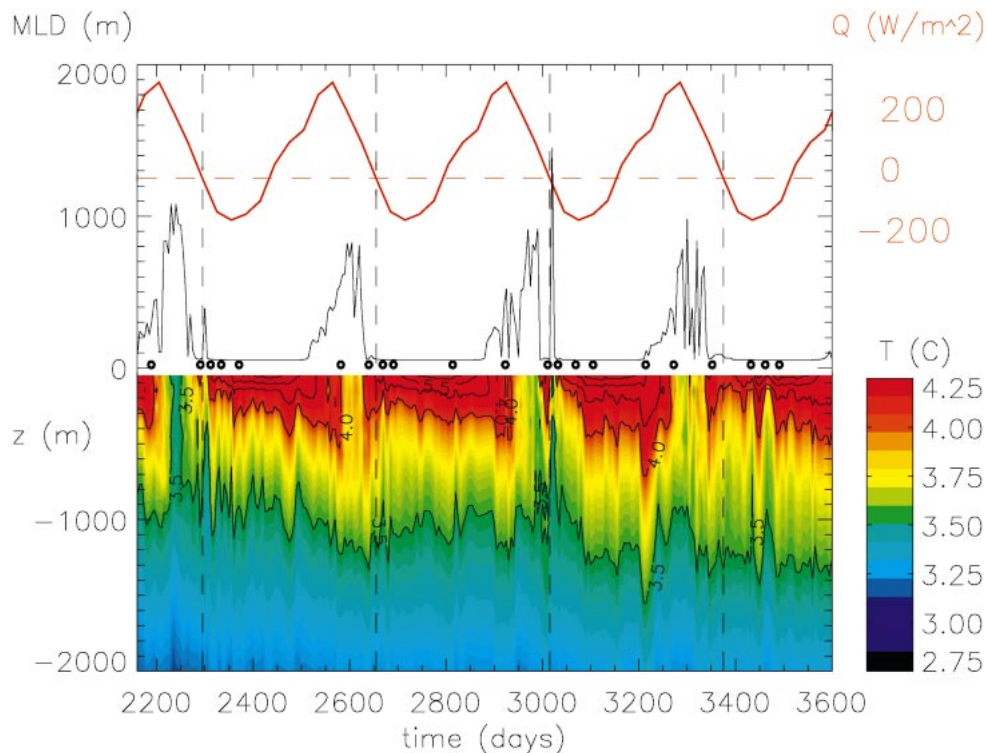
Fig. 13. Characteristics of the equilibrated simulation at the Bravo site (asterisk in Figs. 12a,b): (bottom) time–depth plot of temperature in the upper 2000 m of the water column (colors), (middle), mixed layer depth (black line), and (top) imposed surface heat flux Q (red line). Only the last 4 yr of a 10-yr simulation are shown. The dashed, vertical lines are guides to the eye marking the onset of summer ($Q < 0$). Circles denote Irminger Current eddies passing the Bravo site.

After a spinup period of several years the flow does indeed equilibrate. The basin-averaged temperature profile in year 10 is slightly warmer than T_{ref} and hardly changes over the last couple of years of the simulation. A time–depth plot of the temperature at the Bravo site is presented in the lower panel of Fig. 13, for the last four years of the simulation. The top and middle panels show the local surface heat flux (red) and mixed layer depth (black). The latter is defined as the depth at which the temperature is 0.025°C lower than the local surface temperature (equivalent to a 0.005 kg m^{-3} change in density). In winter, convection is seen to reach a depth of about 1000 m, while in summer the upper ocean restratifies over roughly 750 m. In line with the observations (Lilly et al. 1999) the deepest mixed layers occur at the end of March (around day 80 of each year). Clearly, seasonal variations in the temperature and mixed layer depth are not determined by the atmospheric forcing alone. While the surface heat flux does not change sign before mid-May (vertical dashed lines in Fig. 13), the restratification starts before that date as is clear from the shoaling mixed layer. The restratification is due to eddies arriving from the west coast of Greenland (the signatures of several passing eddies are annotated by circles in Fig. 13).

The presence of anticyclonic, warm-core eddies is

expected to result in heterogeneous convection: the downward doming of isopycnals at their centers tends to hinder convection locally (Legg and McWilliams 2001). As an example, the convective modification of an Irminger Current eddy shed in mid-January is shown in Fig. 14. Its surface temperature decreases by 1.2°C in a month. A mixed layer of about 450 m develops at its core (not shown), while convection reaches 550 m outside the eddy at that time. Despite the strong cooling, the eddy remains coherent, again in line with the anticyclonic eddies in the simulations discussed by Legg and McWilliams (2001). Such winter-modified eddies have also been observed, for example, during the 1997 occupation of the AR7W section (Pickart et al. 2002), and in January 1998 (Lilly et al. 2003). The latter Irminger Current eddy, found in the western Labrador Sea, was surveyed in detail and clearly displayed a well-mixed core about 500 m deep.

For more moderate forcing (using a basin-averaged heat loss of $\overline{Q} = +38$ W m^{-2}), the simulated seasonal variations are similar in nature to those for the standard case discussed above. However, the characteristics of the winter and summer state are different. For example, the mixed layer depth at the Bravo site reduces substantially to about 450 m. Since the surface cooling is weaker, the boundary current remains relatively warm
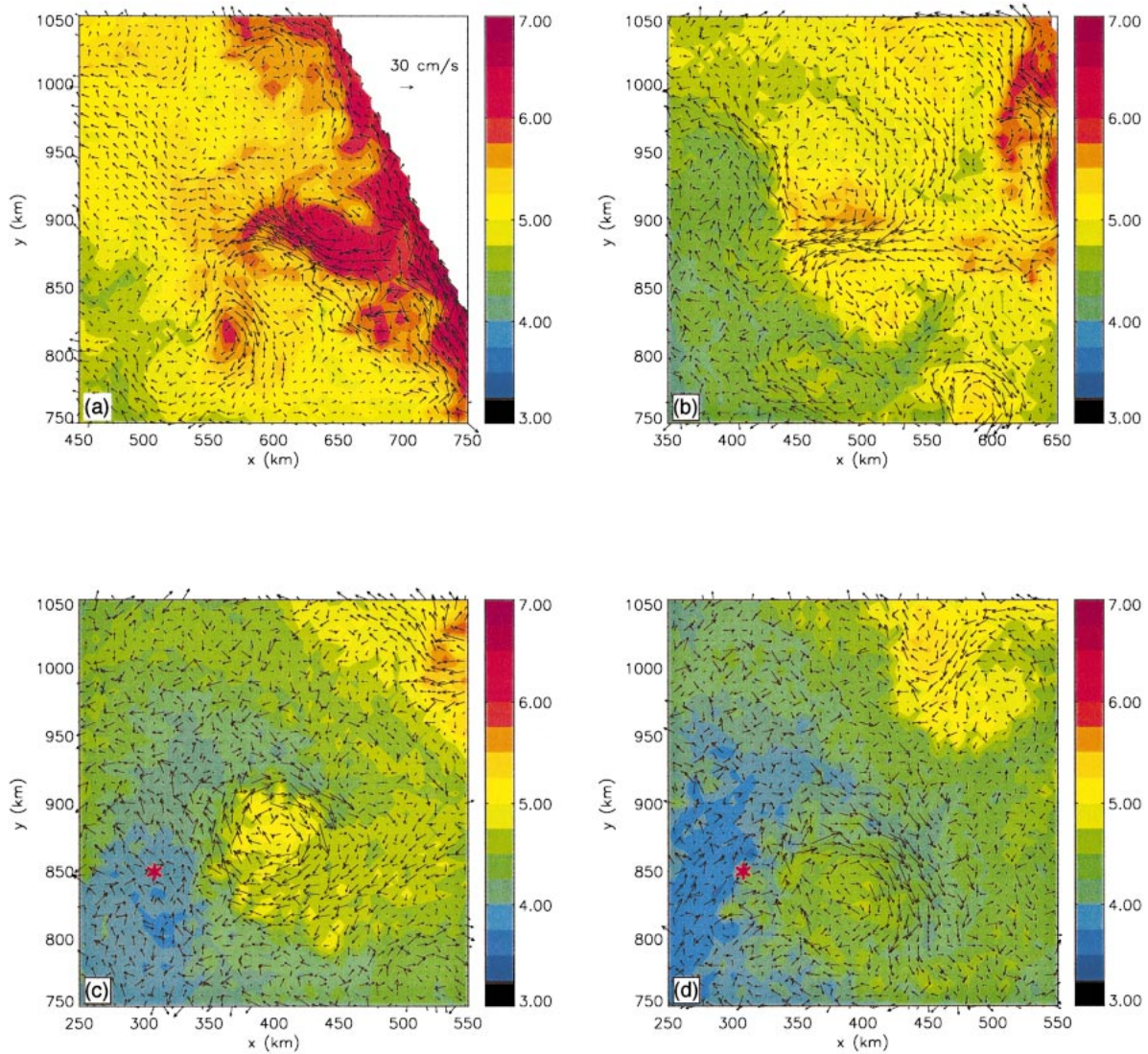
FIG. 14. (a)–(d) Near-surface temperature (°C; colors) and velocity (arrows) of an eddy shed in winter (snapshots are 10 days apart, starting on 10 Jan of year 10 of the simulation). The Bravo site is marked in red in (c) and (d). Note that the plotted subdomain follows the path of the eddy.

in winter so that the initial heat anomaly of newly shed eddies is larger than for the standard simulation. In addition, less of that heat anomaly is released to the atmosphere before the eddies arrive at the Bravo site. As a result, the basin-averaged temperature profile at the end of this 10-yr simulation is clearly warmer than for the standard case.

It can be shown that the lateral heat flux provided by the Irminger Current eddies is crucial to obtain a realistic equilibrium state in the model simulations. By configuring the model bathymetry to have a wide slope along the entire coast of Greenland, it is possible to perform a simulation with a stable boundary current. In this case, restratification occurs only near the surface and is in phase with the surface heat flux. Convection reaches the bottom (at 3000 m) by the third winter,

and in subsequent winters the temperature in the basin interior decreases steadily. In other words, the observed density contrast between the interior of the Labrador Sea and the Irminger Current is not consistent with a more stable boundary current. The interplay between the density of convected water masses and the stability of the boundary current was discussed by Spall (2004), where it was demonstrated that the temperature contrast between the boundary current and the convected water masses in the interior of idealized marginal seas increased to the point that lateral eddy fluxes from the boundary current can balance surface cooling in the interior. These findings imply that Labrador Sea water would be colder and more dense if there were not such a sharp constriction in the topography along the west coast of Greenland.

6. Summary and discussion

Our modeling study has demonstrated the importance of eddies shed by the Irminger Current in the restratification of the Labrador Sea after deep convection. The characteristics of the eddies generated within our idealized model configuration agree well with the existing observations (e.g., Lilly et al. 2003; Prater 2002). The eddy formation process was found to be of mixed type and is governed by the characteristics of the bathymetry near the west coast of Greenland. These Irminger Current eddies are far more effective than rim current eddies [geostrophic eddies shed by a baroclinic rim current along an interior front; Jones and Marshall (1997)] in restratifying a convected region modeled after the observed state of the Labrador Sea at the end of winter (Pickart et al. 2002). In the model simulation, the heat transported into the Labrador Sea interior by the Irminger Current eddies is sufficient to balance the net annual heat loss to the atmosphere and create a fairly realistic equilibrated state. Estimates based on observational data confirm the large impact of Irminger Current eddies on the Labrador Sea heat budget. The properties of the equilibrated state, including the mixed layer depth and basin-averaged temperature profile, depend on a subtle interplay between the surface heat flux and the lateral heat transport provided by the eddies.

According to the observations, there is a clear seasonal signal in the magnitude of the surface eddy kinetic energy (EKE) found near the west coast of Greenland (Fig. 1) with a maximum in late winter/early spring (White and Heywood 1995; Prater 2002). Lilly et al. (2003) attributed this seasonal variability to variations in the number of eddies that is shed by the Irminger Current. In the model simulations presented by Eden and Böning (2002) the variations in EKE are in phase with those in the strength of the boundary current (their Fig. 14). Removal of the seasonal cycle in the wind stress did not lead to a change in the magnitude of the EKE signal in their simulations. By contrast, the seasonality of both the Irminger Current transport and the EKE signal faded away when the heat flux was taken to be constant as well. A plausible explanation for this behavior is that the strong cooling in winter increases the temperature contrast between the boundary current and the Labrador Sea interior so that the boundary current accelerates (Spall 2004).

Our simulations support this explanation. While the EKE signal is fairly constant over the year in the absence of surface forcing, a clear seasonal cycle appears with the introduction of the variable surface heat flux (section 5). In the equilibrium simulation with a stable boundary current, the varying heat flux introduces a pronounced seasonal signal in the strength of the boundary current. In winter, the lateral temperature gradient increases and the Irminger Current becomes stronger, in agreement with the simple theory described in Spall (2004). In the (standard) simulation with an unstable Irminger Current,

this acceleration of the boundary current results in increased eddy shedding. In line with the observations, the the EKE is largest in spring. In the central Labrador Sea, the EKE signal is weaker and lags that near Greenland by a few months, reflecting the propagation of the Irminger Current eddies away from the coast. A similar signal was found by Lilly et al. (2003).

REFERENCES

Böning, C. W., and R. G. Budich, 1992: Eddy dynamics in a primitive equation model: Sensitivity to horizontal resolution and friction. *J. Phys. Oceanogr.,* **22,** 361–381.

Bracco, A., and J. Pedlosky, 2003: Vortex generation by topography in locally unstable baroclinic flows. *J. Phys. Oceanogr.,* **33,** 207–219.

Bush, A. G., J. C. McWilliams, and W. R. Peltier, 1996: The formation of oceanic eddies in symmetric and asymmetric jets. Part II: Late time evolution and coherent vortex formation. *J. Phys. Oceanogr.,* **26,** 1825–1848.

Clarke, R. A., 1984: Transport through the Cape Farewell–Flemish Cap section. *Rapp. V. P. Reun. Cons. Int. Explor.,* **185,** 120–130.

——, and J. C. Gascard, 1983: The formation of Labrador Sea water. Part I: Large-scale processes. *J. Phys. Oceanogr.,* **13,** 1764–1778.

Cuny, J., P. B. Rhines, P. P. Niiler, and S. Bacon, 2002: Labrador Sea boundary currents and the fate of the Irminger Sea Water. *J. Phys. Oceanogr.,* **32,** 627–647.

Dickson, R., J. Lazier, J. Meincke, P. Rhines, and J. Swift, 1996: Long-term coordinated changers in the convective activity of the North Atlantic. *Progress in Oceanography,* Vol. 38, Pergamon, 241–295.

Eden, C., and C. Böning, 2002: Sources of eddy kinetic energy in the Labrador Sea. *J. Phys. Oceanogr.,* **32,** 3346–3363.

Fratantoni, D., 2001: North Atlantic surface circulation during the 1990s observed with satellite-tracked drifters. *J. Geophys. Res.,* **106,** 22 067–22 093.

Jones, H. J., and J. Marshall, 1993: Convection with rotation in a neutral ocean: A study of open ocean deep convection. *J. Phys. Oceanogr.,* **23,** 1009–1039.

——, and ——, 1997: Restratification after deep convection. *J. Phys. Oceanogr.,* **27,** 2276–2287.

Lazier, J. R. N., 1973: The renewal of Labrador Sea Water. *Deep-Sea Res.,* **20,** 341–353.

Legg, S., and J. C. McWilliams, 2001: Convective modifications of a geostrophic eddy field. *J. Phys. Oceanogr.,* **31,** 874–891.

Lilly, J. M., 2002: Observations of the Labrador Sea eddy field. Ph.D. thesis, University of Washington, 242 pp.

——, and P. B. Rhines, 2002: Coherent eddies in the Labrador Sea observed from a mooring. *J. Phys. Oceanogr.,* **32,** 585–598.

——, ——, M. Visbeck, R. Davis, J. R. N. Lazier, F. Schott, and D.

Farmer, 1999: Observing deep convection in the Labrador Sea during winter 1994/95. *J. Phys. Oceanogr.,* **29,** 2065–2098.

——, ——, F. Schott, K. Lavender, J. Lazier, U. Send, and E. D'Asaro, 2003: Observations of the Labrador Sea eddy field. *Progress in Oceanography,* Vol. 59, Pergamon, 75–176.

Marshall, J., and F. Schott, 1999: Open ocean deep convection: Observations, models and theory. *Rev. Geophys.,* **37,** 1–64.

——, A. Adcroft, C. Hill, L. Perelman, and C. Heisey, 1997: A finite-volume, incompressible Navier Stokes model for studies of the ocean on parallel computers. *J. Geophys. Res.,* **102,** 5753–5766.

Orlanski, I., 1976: A simple boundary condition for unbounded hyperbolic flows. *J. Comput. Phys.,* **21,** 251–269.

Pickart, R. S., M. A. Spall, and J. R. N. Lazier, 1997: Mid-depth ventilation in the western boundary current system of the subpolar gyre. *Deep-Sea Res.,* **44,** 1025–1054.

——, D. J. Torres, and R. A. Clarke, 2002: Hydrography of the Labrador Sea during active convection. *J. Phys. Oceanogr.,* **32,** 428–457.

Prater, M. D., 2002: Eddies in the Labrador Sea as observed by profiling RAFOS floats and remote sensing. *J. Phys. Oceanogr.,* **32,** 411–427.

Reynauld, T., A. Weaver, and R. Greatbatch, 1995: Summer mean circulation of the northwestern North Atlantic. *J. Geophys. Res.,* **100,** 779–816.

Rhines, P. B., and J. R. N. Lazier, 1995: A 13-year record of convection and climate change in the deep Labrador Sea. Abstract Report of NOAA Principal Investigator's Meeting, 50–55.

Sathiyamoorthy, S. G., and G. W. K. Moore, 2002: Buoyancy flux at Ocean Weather Station Bravo. *J. Phys. Oceanogr.,* **32,** 458–474.

Smith, S., and F. W. Dobson, 1984: The heat budget at Ocean Weather Station Bravo. *Atmos.–Ocean,* **22,** 1–22.

Spall, M. A., 2004: Boundary currents and water mass transformation in marginal seas. *J. Phys. Oceanogr.,* **34,** 1197–1213.

Stammer, D., and C. Wunsch, 1999: Temporal changes in eddy energy of the oceans. *Deep-Sea Res.,* **46B,** 77–108.

——, C. Böning, and C. Dieterich, 2001: The role of variable wind forcing in generating eddy energy in the North Atlantic. *Progress in Oceanography,* Vol. 48, Pergamon, 289–312.

Visbeck, M. J., J. Marshall, and H. Jones, 1996: Dynamics of isolated convective regions in the ocean. *J. Phys. Oceanogr.,* **26,** 1721–1734.

White, M., and K. Heywood, 1995: Seasonal and interannual changes in the North Atlantic subpolar gyre from *Geosat* and TOPEX/Poseidon altimetry. *J. Geophys. Res.,* **100,** 24 931–24 941.